Computational Materials Science 124 (2016) 420–427

Contents lists available at ScienceDirect

Computational Materials Science

journal homepage: www.elsevier.com/locate/commatsci

Ab-initio investigation of the finite-temperatures structural, elastic, and thermodynamic properties of Ti_3AlC_2 and Ti_3SiC_2

Woongrak Son, Thien Duong, Anjana Talapatra, Huili Gao, Raymundo Arróyave *, Miladin Radovic

Department of Materials Science and Engineering, Texas A&M University, College Station, TX 77843-3123, United States

ARTICLE INFO

Article history:
Received 15 June 2016
Received in revised form 9 August 2016
Accepted 10 August 2016
Available online 24 August 2016

Keywords:
MAX phases
DFT
Elastic constants

ABSTRACT

In this work, we calculate the structural, elastic, thermodynamic properties of Ti_3SiC_2 and Ti_3AlC_2 using a density functional theory (DFT) framework. The vibrational, electronic and quasi-harmonic contributions as well as an anharmonic correction to the total free energy of the system are computed and extrapolated to determine the finite-temperatures properties of the systems. Charge densities, electron localization functions (ELF), the electronic density of states (EDOS) and the vibrational density of states (VDOS) are analyzed in order to deepen our understanding of the interactions giving rise to the calculated properties. Calculated values of Young's modulus, Heat Capacity and Coefficient of Thermal Expansion (CTE) show good agreement with experimental values.

1. Introduction

The $M_{n+1}AX_n$, or MAX phases are ternary carbides or nitrides with a hexagonal crystal structure, wherein the $M_{n+1}X_n$ layers are interleaved with A layers. M is an early transition metal, A is an A-group element, which is mostly 13 and 14 groups and X is carbon or nitrogen. MAX phases exhibit a unique combination of properties arising from their atomic bonding and structural characteristics which situates them on the boundary between metals and ceramic bridging the gap between them [1–6]. Due to the metallic nature of the M and A elements, MAX phases tend to be relatively soft and readily machinable (due to weak M-A bonds), with good thermal shock resistance as well as damage tolerance, and in addition are excellent thermal and electrical conductors. Conversely, being carbides and nitrides they exhibit typical ceramic properties and are good refractory materials, are very stable thermodynamically at high temperatures, have good chemical resistance and have relatively low thermal expansion coefficients. These properties make MAX phases amenable for use in the automotive and aerospace industry [2,3,5].

The '*n*' in the $M_{n+1}AX_n$ phases, denotes the number of M layers sandwiched between the A layers. Researchers have reported M_2AX, M_3AX_2, and M_4AX_3 phases, which refer to the 211, 312, and 413 phases, respectively. In 1967, Ti_3SiC_2 and Ti_3GeC_2 were first synthesized by Jeitschko and Nowotny in powder form [7]; but it wasn't until two decades later that the synthesis of Ti_3AlC_2 by Pietzka and Schuster [8] and that of Ti_3SiC_2 in bulk form by Barsoum and El-Raghy [9] revived interest in this class of materials. In this work, particularly, the 312 MAX phases Ti_3SiC_2 and Ti_3AlC_2 are investigated. The finite-temperatures structural, elastic, and thermodynamic properties of both phases are calculated.

Lane et al. [10] reported on the crystal structures of the Ti_3SiC_2 and Ti_3GeC_2 at finite-temperatures. The anisotropical atomic vibration motion of the Si and Ge are shown from the neutron diffraction with the highest amplitudes along basal planes. Togo et al. [11] reported on the thermal expansion of the Ti_3SiC_2 and Ti_3AlC_2. They found that the volume expansion of the Ti_3SiC_2 is higher than that of the Ti_3AlC_2, and the bulk modulus of Ti_3SiC_2 is higher than that of Ti_3AlC_2. The inversion in ranking in bulk modulus and thermal expansion is rather unexpected as stiffer lattices tend to have smaller thermal expansion coefficients [12], although Togo et al. did not further discuss these findings.

Knowledge of the thermodynamic properties such as the heat capacity of materials can be used to describe the phase stability in multi phase systems, which are important under the synthesis and processing conditions. Duong et al. [13,14] have calculated the finite-temperatures properties for the Ti_2AX (A = Al or Ga and X = C or N) systems. Radovic et al. [15] determined the dependency of elastic properties and damping on temperature for Ti_3SiC_2, Ti_3GeC_2, $Ti_3Si_{0.5}Al_{0.5}C_2$ and Ti_2AlC using resonant ultrasound spectroscopy. They found that the elastic moduli decrease linearly with increasing temperature while the mechanical damping depends weakly on temperature up to ≈1273 K for Ti_3SiC_2, Ti_2AlC and $Ti_3Si_{0.5}Al_{0.5}C_2$, and ≈700 K for Ti_3GeC_2 after which it increases

* Corresponding author at: 218 RDMD, Mail Stop 3123, Texas A&M University, College Station, TX 77843-3123, United States.
E-mail address: rarroyave@tamu.edu (R. Arróyave).

http://dx.doi.org/10.1016/j.commatsci.2016.08.015
0927-0256/

significantly. Amini et al. [16,17] used the Vickers hardness and ultrasound experiments to report the mechanical properties of Ti_2SC and Cr_2GeC. Other than these instances, very little thermodynamic data on MAX phases is available, which exemplifies the need for more such calculations and experiments.

In this work, we calculate the structural, elastic, thermodynamic properties of Ti_3SiC_2 and Ti_3AlC_2 using a density functional theory (DFT) framework [18]. The vibrational and electronic contributions and anharmonic correction to the total free energy of the system are computed and extrapolated to determine the finite-temperatures properties of the systems. Charge densities, electron localization functions (ELF),the electronic density of states (EDOS) and the phonon density of states (PDOS) are analyzed in order to deepen our understanding of the interactions giving rise to the calculated properties.

The organization of this article is as follows: In Section 2, we describe the methodology used to calculate the ground state and finite-temperatures properties and the computational parameters used for the same. In Section 3 we present the results obtained and analyze the electronic structure and vibrational contributions in the materials under consideration. We also discuss the physical factors underlying the results. Finally, Section 4 summarizes the scope of this work and the results obtained.

2. Methodology

2.1. Density Functional Theory (DFT)

The total energy calculation was performed based on Density Functional Theory (DFT), which is implemented in the Vienna Ab-initio Simulation Package (VASP) [19,20]. The Local Density Approximation (LDA) and Generalized Gradient Approximation (GGA) were used for the exchange correlation [21,22]. The Perdew-Burke-Ernzerhof (PBE) is the simplified version of the GGA. The electronic configuration of atoms of titanium, aluminum, silicon and carbon was chosen to be $[Ar]3d^3 4s^1$, $[Ne]3s^2 3p^1$, $[Ne]3s^2 3p^2$ and $[He]2s^2 2p^2$ within the projector augmented-wave (PAW) pseudopotentials formalism. Full relaxations were realized by using the Methfessel-Paxton smearing method [23].

2.2. Elastic properties

The elastic constants were estimated by stress–strain approach where a set of strains ($\varepsilon = \varepsilon_1,\ \varepsilon_2,\ \varepsilon_3,\ \varepsilon_4,\ \varepsilon_5$ and ε_6) is imposed on a crystal structure. If A is the lattice vectors specified in Cartesian coordinates, $\varepsilon_1,\ \varepsilon_2,\ \varepsilon_3$ and $\varepsilon_4,\ \varepsilon_5,\ \varepsilon_6$ are the normal and shear stains, respectively. The deformed lattice vectors are

$$\overline{A} = A\begin{vmatrix} 1+\varepsilon_1 & \frac{\varepsilon_6}{2} & \frac{\varepsilon_5}{2} \\ \frac{\varepsilon_6}{2} & 1+\varepsilon_2 & \frac{\varepsilon_4}{2} \\ \frac{\varepsilon_5}{2} & \frac{\varepsilon_4}{2} & 1+\varepsilon_3 \end{vmatrix}.$$

A set of stresses ($\sigma = \sigma_1,\ \sigma_2,\ \sigma_3,\ \sigma_4,\ \sigma_5$ and σ_6) for the deformed crystals is generated, which is calculated using density functional theory (DFT) methods. From the n set of strains and the resulting stresses, elastic constants are calculated based on Hook's law, as shown below.

$$\begin{vmatrix} C_{11} & \cdots & C_{16} \\ \vdots & & \vdots \\ C_{61} & \cdots & C_{66} \end{vmatrix} = \begin{vmatrix} \varepsilon_{1,1} & \cdots & \varepsilon_{1,n} \\ \vdots & & \vdots \\ \varepsilon_{6,1} & \cdots & \varepsilon_{6,n} \end{vmatrix}^{-1} \begin{vmatrix} \sigma_{1,1} & \cdots & \sigma_{1,n} \\ \vdots & & \vdots \\ \sigma_{6,1} & \cdots & \sigma_{6,n} \end{vmatrix}$$

The mechanical stability is determined by the crystal energy, which contains a quadratic form of strain energy:

$$E = E_0 + \frac{1}{2}V_0\sum_{i,j=1}^{6} C_{ij}\varepsilon_i\varepsilon_j + O(\varepsilon^3) \quad (1)$$

By ensuring that the quadratic form of elastic energy is always positive, the mechanical stability criteria of hexagonal phase are given by:

$$C_{44} > 0, C_{11} > |\ C_{12}\ |,$$
$$(C_{11} + 2C_{12})C_{33} > 2C_{13}^2. \quad (2)$$

2.3. Finite-temperatures elastic properties

After calculating the elastic constants on different volume, the finite-temperatures elastic constants can be derived by the dependence of volume on temperature. The latter can be achieved by fitting the free energy equation to the equilibrium volumes at different temperatures. The finite-temperatures elasticity can be derived as follows [24]:

$$C_{ij}(T) = C_{ij}(V(T)) \quad (3)$$

The calculated elastic constants correspond to the isothermal condition. However, experimentally, the elastic constants are achieved under adiabatic condition. Therefore, we converted the calculated isothermal elastic constants to the adiabatic elastic constants. It can be converted by the Davies's approximation, which relates the isothermal elastic constants to the adiabatic elastic constants by the following equation:

$$C_{ij}^S = C_{ij}^T + \frac{TV\lambda_i\lambda_j}{C_V}, \quad (4)$$

where C_{ij}^S, C_{ij}^T and C_V represents adiabatic elastic constants, isothermal elastic constants and specific heat at constant volume, respectively:

$$\lambda_i = \sum_j \alpha_j C_{ij}^T \quad (5)$$

Anisotropic coefficients of thermal expansion, α_j, can be calculated as: $\alpha_1 = \Lambda_{11},\ \alpha_2 = \Lambda_{22},\ \alpha_3 = \Lambda_{33},\ \alpha_4 = \Lambda_{23},\ \alpha_5 = \Lambda_{13} + \Lambda_{13}$ and $\alpha_6 = \Lambda_{12} + \Lambda_{21}$:

$$\Lambda(T) = R^{-1}\left(\frac{\partial R}{\partial V}\right)\left(\frac{\partial V}{\partial T}\right) \quad (6)$$

$\Lambda(T)$ is an anisotropic tensor of thermal expansion, and R is a 3×3 matrix, which combines three lattice vectors: $R(V) = (a(V),\ b(V),\ c(V))^T$.

2.4. Finite-temperature thermodynamics

The finite-temperatures thermodynamic properties can be derived from the total free energy of a system. In this work, we consider vibrational and electronic contributions and anharmonic correction. The vibrational contribution is obtained by the supercell method, which is implemented in the ATAT package [25]. We calculate force constant tensor of each pair of atoms in the system. We compile all the force constant tensors into the so-called dynamical matrix, which has eigenvalues (frequencies) of the normal modes of oscillation in the system. The phonon density of states (PDOS) can be achieved from the frequencies, and PDOS is related to the vibrational free energy through the statistical mechanics [26,27]:

$$F_{vib}(V,T) = k_B T\int_0^\infty ln[2sinh\left(\frac{h\nu}{2k_B T}\right)]g(\nu)|_V d\nu \quad (7)$$

k_B is Boltzmann's constant, h is Planck's constant, T is temperature, V is the quasi-harmonic volume, v is the frequency and $g(v)|_V$ is the phonon density of states of the structure corresponding to V.

The electronic degrees of freedom affect to the total free energy of a system. The electronic density of states, $n(\varepsilon)$, and the Fermi function, f, are related to the free energy of electrons by the statistical physics as follows:

$$F_{el}(V,T) = E_{el}(V,T) - TS_{el}(V,T) \tag{8}$$

$$E_{el}(V,T) = \int n(\varepsilon)|_V f\varepsilon d\varepsilon - \int^{\varepsilon_F} n(\varepsilon)|_V \varepsilon d\varepsilon \tag{9}$$

$$S_{el}(V,T) = -k_B \int n(\varepsilon)|_V [flnf + (1-f)ln(1-f)]d\varepsilon \tag{10}$$

Wallace developed the anharmonic free energy equation, which is related to the expansion of the crystal potential.

$$F_{anhar} = A_2 T^2 + A_0 + A_{-2} T^{-2} + L \tag{11}$$

$$A_2 = \frac{3k_B}{\Theta}(0.0078 < \gamma > -0.0154) \tag{12}$$

The Gruneisen parameter, γ, and the coefficients are based on an empirical data. The anharmonic free energy is only reasonable in the high temperature region since they ignore the last three terms, which cannot be easily determined. Then, Oganov developed the anharmonic free energy, and extended it to all temperature region. Using thermodynamic perturbation theory he obtained an expression for the anharmonic free energy as a function of temperature:

$$\frac{F_{anhar}}{3nk_B} = \frac{a}{6}\left[\left(\frac{1}{2}\theta + \frac{\theta}{exp(\theta/T)-1}\right)^2 + 2\left(\frac{\theta}{T}\right)^2 \frac{exp(\theta/T)}{(exp(\theta/T)-1)^2} T^2\right] \tag{13}$$

where a is $1/2A_2$ and θ corresponds to the high temperature Harmonic Debye temperature, defined as $\theta = \frac{\hbar}{k_B}\left(\frac{5}{3} < \omega^2 >\right)^{\frac{1}{2}}$.

The total free energy of the system is the summation of the aforementioned energy terms:

$$F_{total}(V,T) = E_{0K}(V) + F_{vib}(V,T) + F_{el}(V,T) + F_{anhar}(V,T) \tag{14}$$

where $E_{0K}(V)$ is the zero-temperature energy at each quasi-harmonic volume.

Thermodynamic properties can be calculated using the total free energy:

$$S = -\frac{\partial F(T)}{\partial T},\ C_P = T\frac{\partial S}{\partial T}. \tag{15}$$

3. Results and discussion

3.1. Ground state calculation

The Ti_3SiC_2 and Ti_3AlC_2 phases form into a nano-layer and hexagonal structure with the space group of P63/mmc, and they are shown in Fig. 1. The ground state calculation is optimized by the self-consistent calculation, which is based on density functional theory [18,28]. The calculations were performed with LDA and GGA. The results are given in Table 1, which agree well with experimented values [29,30], and other calculated values. We export calculated properties from the Mateirlas Project (www.materialsproject.org) [31], which is open dataset to uncover ground state properties of all known inorganic materials. The experimental lattice parameters lie within the LDA-GGA lattice parameters range. The calculated lattice parameters shows that the LDA results

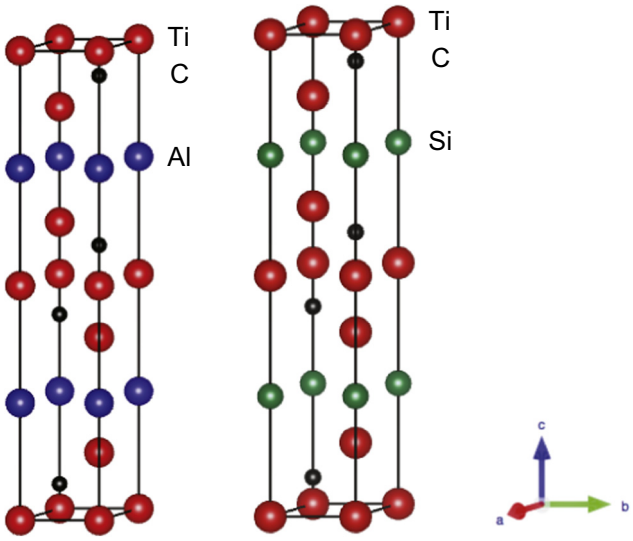

Fig. 1. Crystal structure of the (a) Ti_3AlC_2 and (b) Ti_3SiC_2.

Table 1
Structural properties of Ti_3AlC_2 and Ti_3SiC_2.

Alloy	Type	Potential	Lattice Parameters		
			a(A)	b(A)	c(A)
Ti_3AlC_2	Calc.	GGA	3.083	3.083	18.652
		LDA	3.070	3.070	18.331
	Calc. (Ref. 31)	GGA	3.081	3.081	18.679
	Exp. (Ref. 27)		3.072	3.072	18.415
Ti_3SiC_2	Calc.	GGA	3.077	3.077	17.715
		LDA	3.028	3.028	17.453
	Calc. (Ref. 31)	GGA	3.073	3.073	17.756
	Exp. (Ref. 28)		3.065	3.065	17.623

underestimate lattice parameter with a discrepancy of ~1.21%, and the GGA results overestimate lattice parameter with a discrepancy of ~0.39%. The GGA results have a smaller discrepancy with experiments and in the remaining of the article, we will present results with GGA calculations. The substitution of Al with Si mostly affects to the decreasing c lattice parameter value (5.02%) than the decreasing a lattice parameter value (0.19%). The results suggest that the substitution of aluminum with silicon mostly affects the c lattice parameter. The decreasing lattice parameters of Ti_3SiC_2 consistent with the fact that lower atomic volume of the silicon than that of the aluminum.

Fig. 2 shows the (100) plane view of charge density of the Ti_3AlC_2 and Ti_3SiC_2. The bader analysis, given in Table 2, shows the total charge associated with each atom and charge transfer of each atom. The amount of the charge transfer of each M, A and X elements, is 0.01, 0.22 and 0.07, respectively, when aluminum is substituted with silicon. The charge density provides a measure of the strength of the ionic bond so that Ti_3SiC_2 has stronger ionic bond than Ti_3AlC_2. The strong M-A bonds in Ti_3SiC_2 result to a decreased c lattice parameter value. Fig. 3 shows the (100) plane view of electron localization function (ELF) data of the Ti_3AlC_2 and Ti_3SiC_2 [32]. ELF value is scaled in the range of 0–1, and provides a (very) qualitative picture of the bonding character within an electronic charge density distribution (in a lattice). The spherical shape of X represents more ionic like bond. The z-Directional localized shape of A represents more covalent like bond. The covalent bond of A elements is localized along the z direction so that it affects mostly the c lattice parameter.

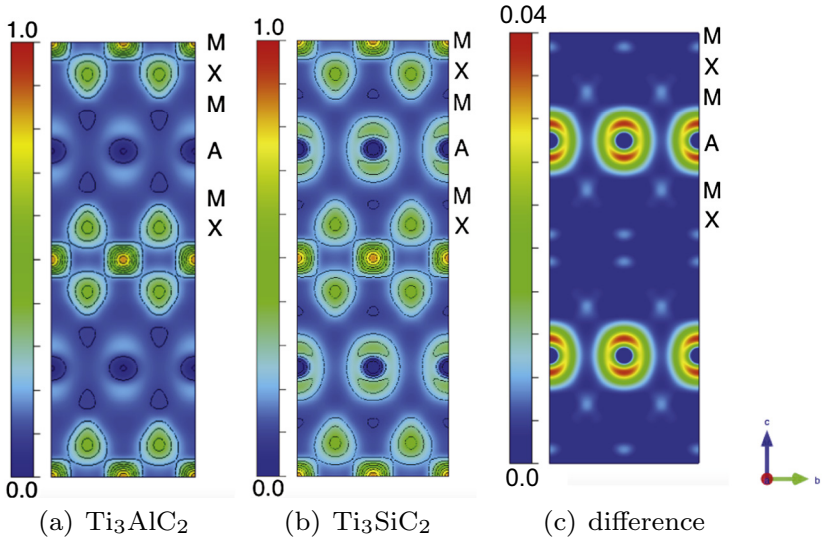

Fig. 2. (100) Plane view of Charge Density for the (a) Ti_3AlC_2, (b) Ti_3SiC_2 and (c) their difference.

Table 2
Calculated total charge (charge transfer) of Ti_3AlC_2 and Ti_3SiC_2 obtained from Bader analysis.

	Ti (d3s1)	C (s2p2)	Al (s2p1), Si (s2p2)
Ti_3AlC_2	1.905 (−2.095)	6.565 (+2.565)	4.155 (+1.155)
Ti_3SiC_2	1.883 (−2.117)	6.488 (+2.488)	5.375 (+1.375)
	Ti (total)	Al & Si (total)	C (total)
Ti_3AlC_2	11.43	26.26	8.31
Ti_3AlC_2	11.3	25.95	10.75
	% Ti	% C	% Al, Si
Ti_3AlC_2	24.85	57.01	18.14
Ti_3SiC_2	23.50	54.10	22.40

Fig. 4 shows the electron density of states of the Ti_3AlC_2 and Ti_3SiC_2. The DOS at the Fermi level mostly dependent on the DOS of titanium, in both of the Ti_3AlC_2 and Ti_3SiC_2. The calculated DOS reported by Zhou et al. [33] also shows that the DOS at Fermi level mostly dependent on the DOS of titanium, in both of the Ti_3AlC_2 and Ti_3SiC_2. The Ti-Si bond is stronger than Ti-Al bond, and the titanium of Ti_3AlC_2 has more electrons than the titanium of Ti_3SiC_2 as shown in bader analysis. It agrees well with the DOS at Fermi level: 2.81 and 2.14 for Ti_3AlC_2 and Ti_3SiC_2, respectively.

3.2. Finite temperature calculations

The elastic constants were calculated using stress-strain approach. The elastic moduli of hexagonal structures were estimated based on Voigt's approximation. According to the Voigt's approximation, the bulk, shear and Young's modulus are calculated as follows [36]:

$$B_V = \frac{2(C_{11}+C_{12})+4C_{13}+C_{33}}{9}, \tag{16}$$

$$G_V = \frac{M+12C_{44}+12C_{66}}{30}, \tag{17}$$

B is bulk modulus, G is shear modulus, E is Young's modulus. Young's modulus E was obtained by the following formulas:

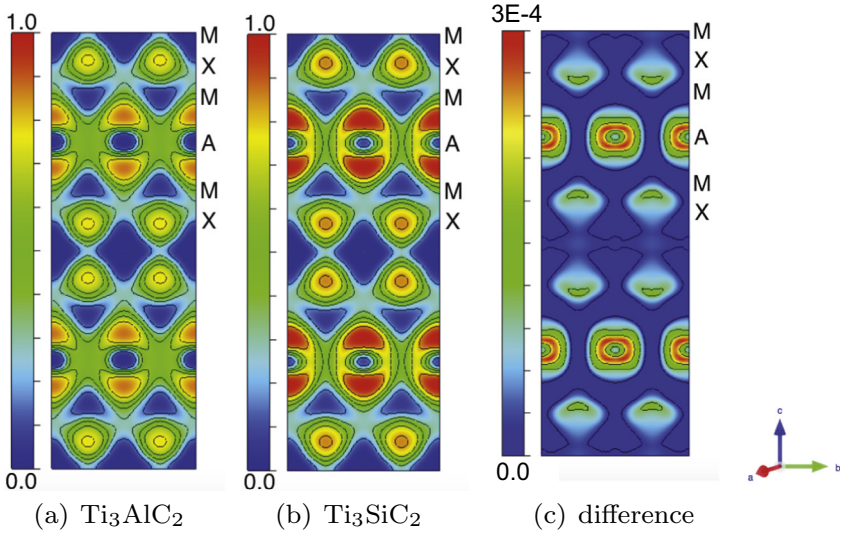

Fig. 3. (100) Plane view of Electron Localization Function (ELF) for the (a) Ti_3AlC_2, (b) Ti_3SiC_2 and (c) their difference.

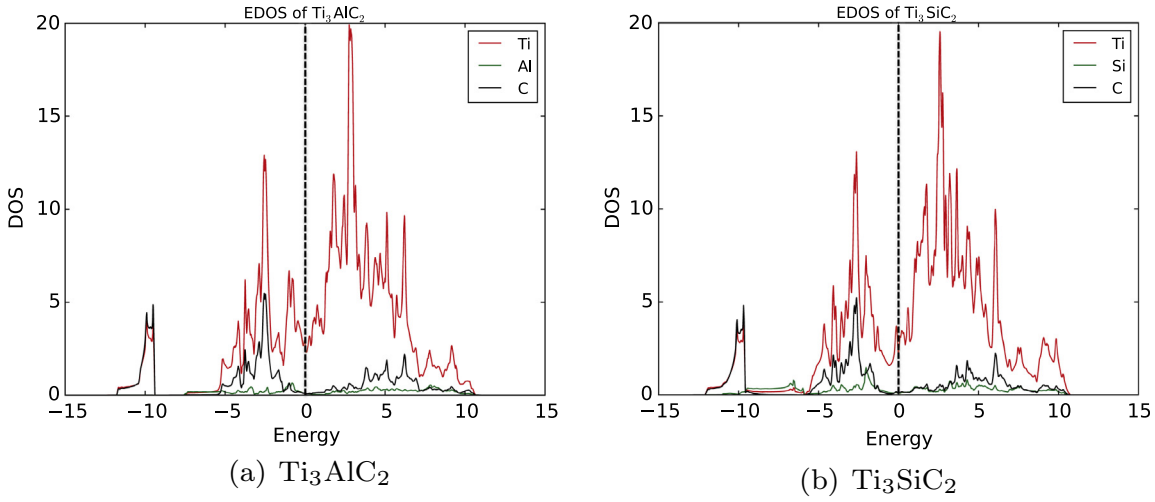

Fig. 4. Electron Density of States of the (a) Ti_3AlC_2 and (b) Ti_3SiC_2.

$$E = \frac{9BG}{3B + G} \tag{18}$$

Table 3 and Fig. 5 show the calculated elastic constants of Ti_3AlC_2 and Ti_3SiC_2. The hexagonal symmetry of the MAX phases result in anisotropic elastic constants (C_{11} and C_{33}). Both of the Ti_3AlC_2 and Ti_3SiC_2 are elastically stiffer along the a direction than along the c direction, and this agrees well with the calculated elastic constants reported by Wang and Zhou [37], and the Materials Project [31]. The substitution of Al with Si highly increases C_{33} to a larger extent than C_{11}, consistent with the fact that A-site substitution tends to affect in greater degree bonding along the c axis. The bulk and Young's modulus of Ti_3AlC_2 and Ti_3SiC_2 on

Table 3
Elastic constants, bulk modulus (B), shear modulus (G), and Young's modulus (E)

Phase	C_{11}	C_{33}	C_{44}	C_{12}	C_{13}	B	G	E	
Ti_3AlC_2	355.45	292.89	119.03	84.63	76.03	163.35	125.47	299.68	
	355.15	296.11	114.5	74.71	69.1	159.14	126.43		(Ref. 31)
Ti_3SiC_2	370.47	349.71	155.43	97.22	112.11	192.61	140.11	338.31	
	362.00	349.64	149.03	89.39	100.86	184.07	138.92		(Ref. 31)

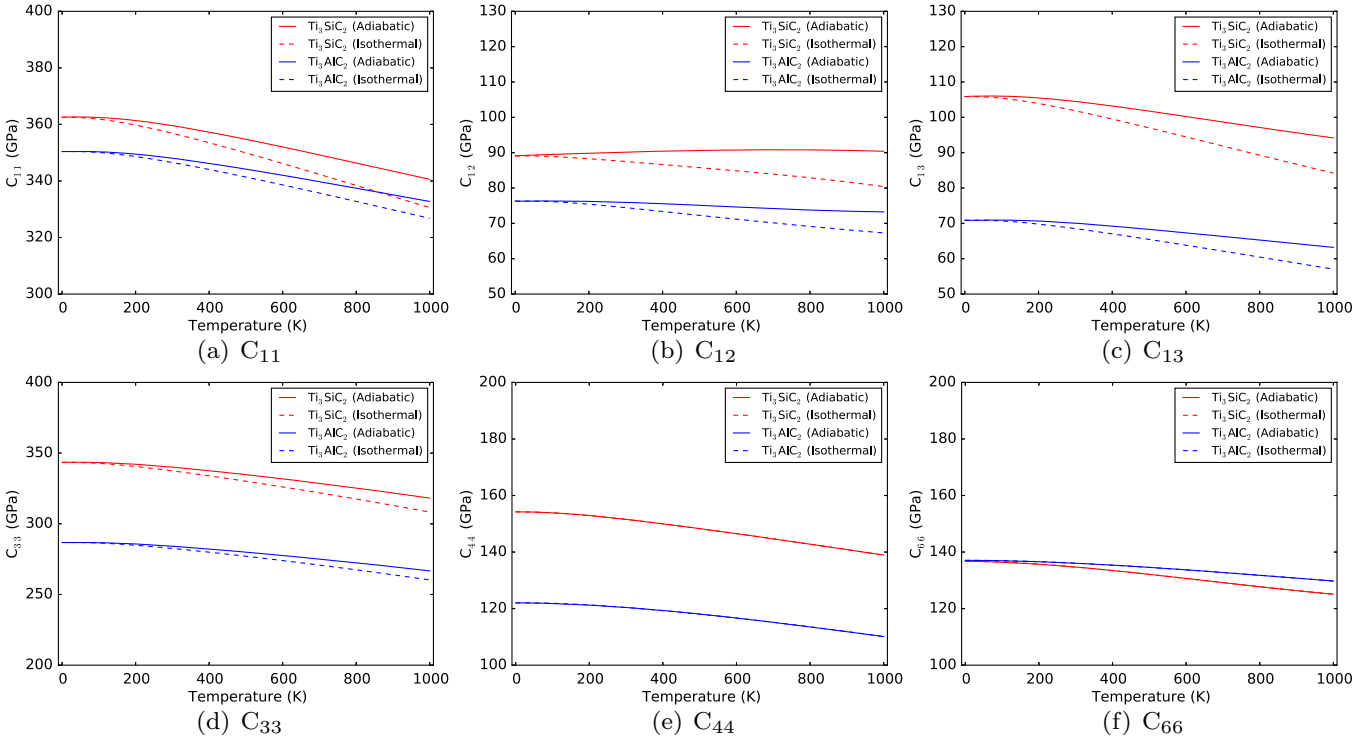

Fig. 5. Adiabatic and isothermal elastic constants for Ti_3AlC_2 and Ti_3SiC_2.

finite-temperatures are compared in Fig. 6. The (low temperature) calculated bulk modulus agrees well with the experimented values: 185 [34] and 187 GPa [34] for Ti_3SiC_2 and 156 [38] and 165 GPa [34] for Ti_3AlC_2. The calculated Young's modulus agrees well with the experimented values reported by Radovic et al. [15], Wang and Zhou [35] and Finkel et al. [34]. The Ti_3SiC_2 has higher bulk modulus and Young's modulus than those of the Ti_3AlC_2.

Generally, as mentioned above, the elastic modulus and thermal expansion are inversely related [12]. However, the Ti_3SiC_2, which has higher elastic modulus than Ti_3AlC_2, softens faster than Ti_3AlC_2 with increasing temperature. The bulk modulus gap between Ti_3SiC_2 and Ti_3AlC_2 at ground state is 27.40 GPa, and at 1000 (K) is 25.03 GPa. The Young's modulus gap between the Ti_3SiC_2 and Ti_3AlC_2 at ground state is 34.22 GPa, and at 1000 (K) is 24.71 GPa. The Coefficient of Thermal Expansion (CTE) of Ti_3AlC_2 and Ti_3SiC_2 are compared in Fig. 7(a). The CTE of Ti_3SiC_2 is higher than that of Ti_3AlC_2. The calculations for Ti_3SiC_2 overestimates the experimentally determined CTE by Zinkle [39].

The calculated thermal expansion of a and c lattice agrees well with experimented values reported by Scabarozi et al. [40]. The calculated a lattice parameter of Ti_3SiC_2 below ~650 K is lower than that of Ti_3AlC_2, however, the thermal expansion of the Si is higher than the Al, and a lattice parameter of the Ti_3SiC_2 is higher than that of the Ti_3AlC_2 above ~650 K. Not surprisingly, there is a certain measure of anisotropy in the thermal expansion tensor. The thermal expansion of a lattice, α_a, and c lattice, α_c of Ti_3SiC_2 are 9.1 (10^{-6} K^{-1}) and 11.0 (10^{-6} K^{-1}), respectively. The thermal expansion of α_a and α_c of Ti_3AlC_2 are 8.2 (10^{-6} K^{-1}) and 11.6 (10^{-6} K^{-1}). The A element mostly vibrates along a direction, which agrees well with the anisotropic atomic vibration of A element with highest frequency within basal plane reported by Lane et al. [10]. The Ti_3AlC_2 compound is clearly more anisotropic (in terms of lattice thermal expansion) than Ti_3SiC_2, and this may be related to the different bond strengths when Si substitutes Al.

The total and partial phonon density of states of the are shown in Fig. 8 in good agreement with the calculated phonon density of states reported by Togo et al. [11]. The partial phonon density of states were investigated to study thermal expansion of the Ti_3SiC_2 and Ti_3AlC_2. The phonon DOS of the Ti and C show similarity in both of the Ti_3SiC_2 and Ti_3AlC_2 phases. Both of the phonon DOS of the Al and Si have low frequencies wherein acoustic region (under 15 THz). However, the area under the curve of phonon DOS of Si and Al are, respectively, 6.40 and 3.89. The higher phonon DOS in acoustic region of the silicon than that of the aluminum agrees well with the calculated thermal expansion coefficient and calculated lattice parameters on finite-temperatures as shown in Fig. 8.

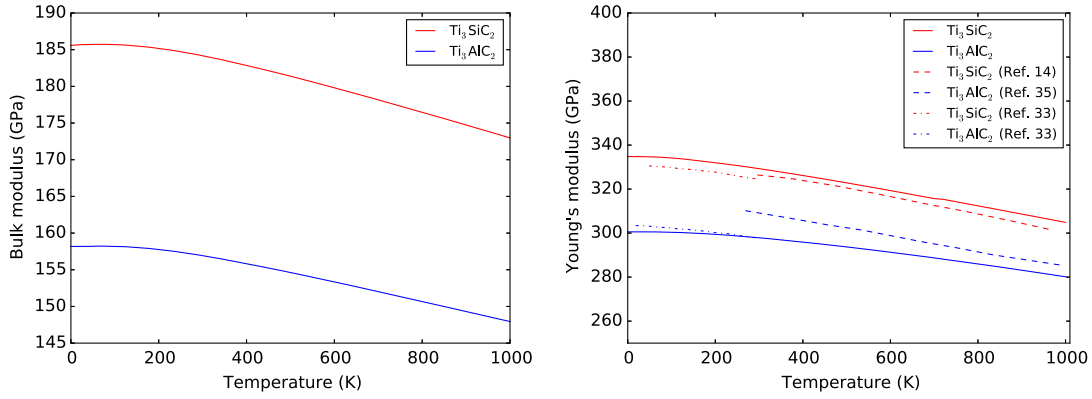

(a) Bulk modulus (b) Young's modulus

Fig. 6. (a) The Bulk and (b) Young's modulus of Ti_3AlC_2 and Ti_3SiC_2 as a function of temperature. Both of the Bulk and Young's modulus are calculated using adiabatic elastic constants. The calculated Young's modulus is compared to the experimental value of Young's modulus reported by Radovic et al. [15], Finkel et al. [34] and Wang and Zhou [35].

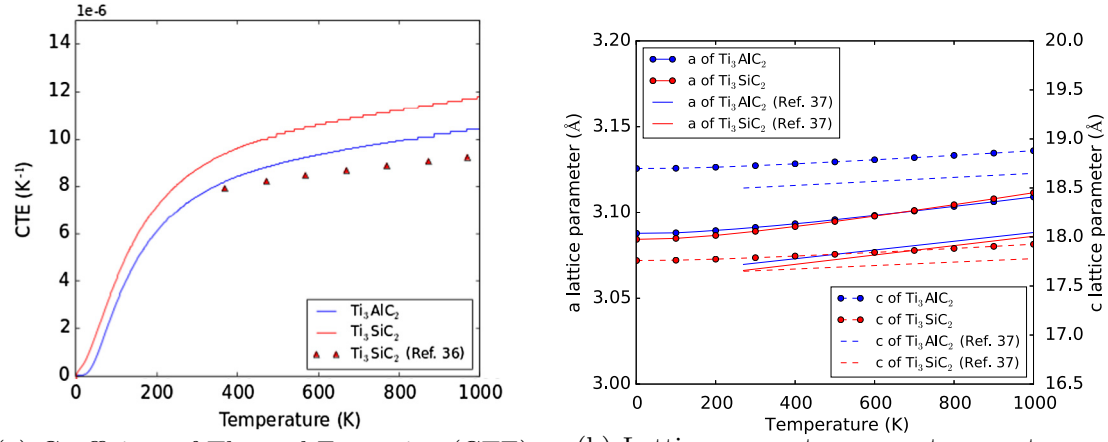

(a) Coefficient of Thermal Expansion (CTE) (b) Lattice parameter versus temperatures

Fig. 7. Coefficient of Thermal Expansion (CTE) of the Ti_3SiC_2 and Ti_3AlC_2. The calculated CTE of Ti_3SiC_2 is compared to the experimental value of CTE reported by Zinkle [39]. The calculated lattice parameters versus temperatures are compared to the experimental value of lattice parameters reported by Scabarozi et al. [40].

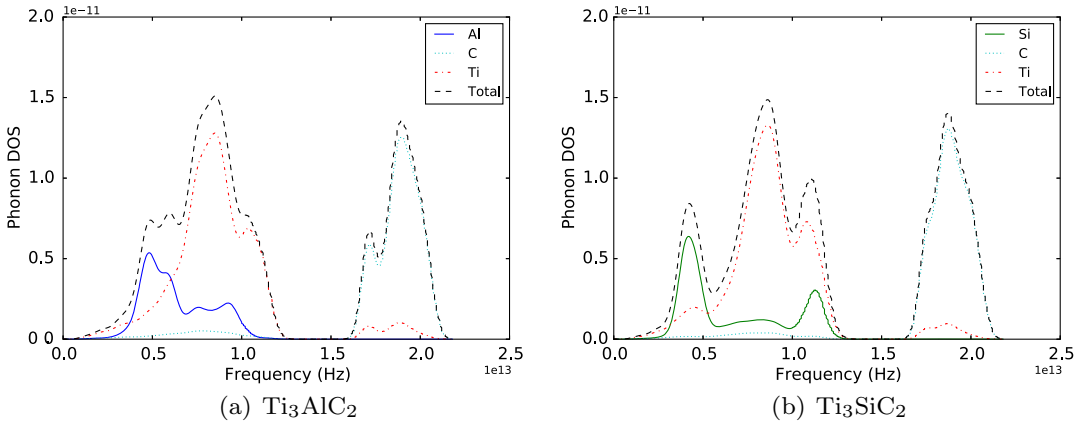

Fig. 8. Total and partial Phonon Density of States (PDOS) of (a) Ti_3AlC_2 and (b) Ti_3SiC_2. The dashed, dashed-dotted and dotted curves denote total, Ti and C, respectively, and the solid line denotes Al and Si.

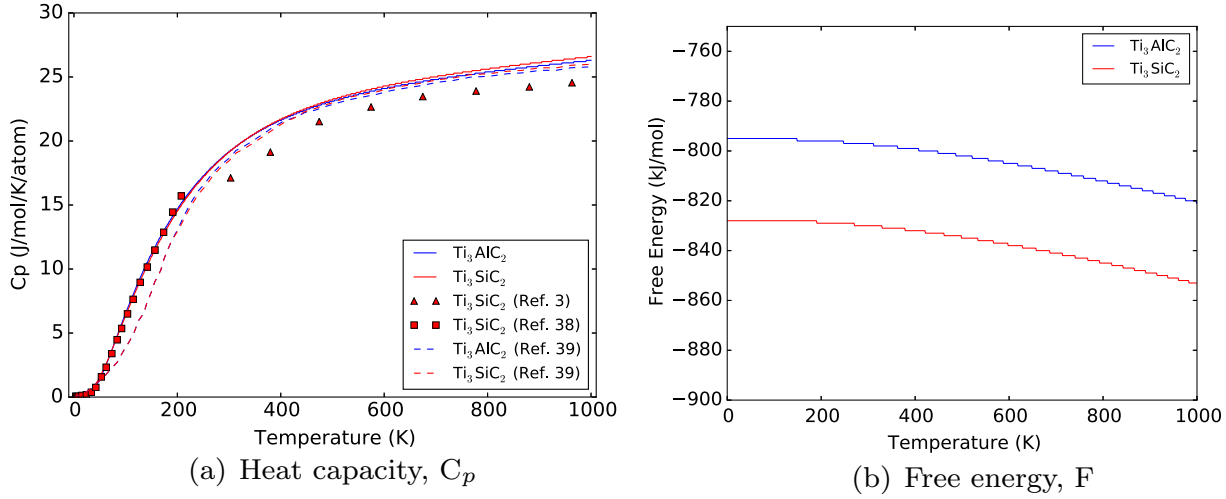

Fig. 9. (a) Heat capacities and (b) free energies as a function of temperature. The red line and blue line denote C_p of Ti_3SiC_2 and Ti_3AlC_2, respectively. For the comparison, the square [3] and triangle [41] depict the experimental values of C_p of Ti_3SiC_2 below 250 K and above 300 K, respectively. The calculated heat capacities are also compared to other computational results reported by Ali et al. [42]. (For interpretation of the references to color in this figure legend, the reader is referred to the web version of this article.)

The thermodynamic properties of Ti_3AlC_2 and Ti_3SiC_2 are shown in Fig. 9. The thermodynamic calculation considers vibrational, electronic and anharmonic contributions. Below 250 K, the calculated heat capacity of Ti_3SiC_2 agrees well with experimented values reported by Drulis et al. [41]. Above 300 K, the calculations slightly overestimate the heat capacity than experiments [3]. The heat capacity of both of the Ti_3AlC_2 and Ti_3SiC_2 are identical, which agrees well with other calculation reported by Ali et al. [42]. The heat capacity was calculated from the free energy as a function of temperature as shown in Eq. 15. It is resulted by the identical vibrational, electronic and anharmonic contributions of both of the Ti_3AlC_2 and Ti_3SiC_2 phases.

4. Conclusions

The structural, elastic and thermodynamic properties of Ti_3AlC_2 and Ti_3SiC_2 were investigated in this study. The calculated results of those properties of Ti_3AlC_2 and Ti_3SiC_2 agree well with the experimental data. The calculated results shows the anisotropic properties of Ti_3AlC_2 and Ti_3SiC_2. The substitution of Al with Si highly effect to the c directional properties, such as lattice parameter and elastic constants. The directly related elastic modulus and thermal expansion is investigated with the finite-temperatures elastic modulus and phonon density of states. The thermodynamic properties were calculated with the vibrational, electronic and anharmonic contributions. We investigated the thermodynamic properties (free energy, entropy and heat capacity) of Ti_3AlC_2 and Ti_3SiC_2 on finite-temperatures.

Acknowledgments

This work was supported by the grant NSF-DMR-1410983. AT acknowledges support from DMR-0844082, while TD acknowledges support from DOE (through LLNL) under contract DE-AC52-07NA27344. First-principles calculations were carried out in the Texas A&M Supercomputing Facility at Texas A&M University.

References

[1] M.W. Barsoum, MAX Phases: Properties of Machinable Ternary Carbides and Nitrides, John Wiley & Sons, 2013.
[2] M. Radovic, M.W. Barsoum, Max phases: bridging the gap between metals and ceramics, Am. Ceram. Soc. Bull. 92 (3) (2013) 20–27.

[3] M.W. Barsoum, The M N + 1 AX N phases: a new class of solids: thermodynamically stable nanolaminates, Prog. Solid State Chem. 28 (1) (2000) 201–281.
[4] M.W. Barsoum, M. Radovic, Mechanical properties of the MAX phases, in: K.H. J. Buschow, R. Cahn, M. Flemings, B. Ilschner, E. Kramer, S. Mahajan, P. Veyssiere (Eds.), Encyclopedia of Materials: Science and Technology, Elsevier, Amsterdam, 2004, pp. 1–16.
[5] M.W. Barsoum, M. Radovic, Elastic and mechanical properties of the max phases, Ann. Rev. Mater. Res. 41 (2011) 195–227.
[6] Z. Sun, Progress in research and development on MAX phases: a family of layered ternary compounds, Int. Mater. Rev. 56 (3) (2011) 143–166.
[7] W. Jeitschko, H. Nowotny, Die kristallstruktur von Ti_3SiC_2–ein neuer Komplexcarbid-Typ, Monatshefte für Chem. verwandte Teile anderer Wissenschaften 98 (2) (1967) 329–337.
[8] M.A. Pietzka, J.C. Schuster, Phase equilibria in the quaternary system Ti-Al-C-N, J. Am. Ceram. Soc. 79 (9) (1996) 2321–2330.
[9] M.W. Barsoum, T. El-Raghy, Synthesis and characterization of a remarkable ceramic: Ti_3SiC_2, J. Am. Ceram. Soc. 79 (7) (1996) 1953–1956.
[10] N.J. Lane, S.C. Vogel, M.W. Barsoum, High-temperature neutron diffraction and the temperature-dependent crystal structures of the MAX phases Ti_3SiC_2 and Ti_3GeC_2, Phys. Rev. B 82 (17) (2010) 174109.
[11] A. Togo, L. Chaput, I. Tanaka, G. Hug, First-principles phonon calculations of thermal expansion in Ti_3SiC_2, Ti_3AlC_2, and Ti_3GeC_2, Phys. Rev. B 81 (17) (2010) 174301.
[12] V. Milman, B. Winkler, M. Probert, Stiffness and thermal expansion of ZrB2: an ab initio study, J. Phys.: Condens. Matter 17 (13) (2005) 2233.
[13] T. Duong, S. Gibbons, R. Kinra, R. Arróyave, Ab-initio approach to the electronic, structural, elastic, and finite-temperature thermodynamic properties of Ti_2AX (A = Al or Ga and X = C or N), J. Appl. Phys. 110 (9) (2011) 093504.
[14] T.C. Duong, N. Singh, R. Arróyave, First-principles calculations of finite-temperature elastic properties of Ti_2AlX (X = C or N), Comput. Mater. Sci. 79 (2013) 296–302.
[15] M. Radovic, M. Barsoum, A. Ganguly, T. Zhen, P. Finkel, S. Kalidindi, E. Lara-Curzio, On the elastic properties and mechanical damping of Ti_3SiC_2, Ti_3GeC_2, $Ti_3Si_{0.5}Al_{0.5}C_2$ and Ti_2AlC in the 300–1573 K temperature range, Acta Mater. 54 (10) (2006) 2757–2767.
[16] S. Amini, M.W. Barsoum, T. El-Raghy, Synthesis and mechanical properties of fully dense Ti_2Sc, J. Am. Ceram. Soc. 90 (12) (2007) 3953–3958.
[17] S. Amini, A. Zhou, S. Gupta, A. DeVillier, P. Finkel, M.W. Barsoum, Synthesis and elastic and mechanical properties of Cr_2GeC, J. Mater. Res. 23 (08) (2008) 2157–2165.
[18] W. Kohn, L.J. Sham, Self-consistent equations including exchange and correlation effects, Phys. Rev. 140 (4A) (1965) A1133.
[19] G. Kresse, J. Furthmüller, Efficient iterative schemes for ab initio total-energy calculations using a plane-wave basis set, Phys. Rev. B 54 (1996) 11169–11186, http://dx.doi.org/10.1103/PhysRevB.54.11169.
[20] G. Kresse, J. Furthmüller, Efficiency of ab-initio total energy calculations for metals and semiconductors using a plane-wave basis set, Comput. Mater. Sci. 6 (1) (1996) 15–50, http://dx.doi.org/10.1016/0927-0256(96)00008-0.
[21] A.D. Becke, A new mixing of hartree–fock and local density-functional theories, J. Chem. Phys. 98 (2) (1993) 1372–1377.
[22] J.P. Perdew, J. Chevary, S. Vosko, K.A. Jackson, M.R. Pederson, D. Singh, C. Fiolhais, Atoms, molecules, solids, and surfaces: applications of the generalized gradient approximation for exchange and correlation, Phys. Rev. B 46 (11) (1992) 6671.
[23] M. Methfessel, A.T. Paxton, High-precision sampling for Brillouin-zone integration in metals, Phys. Rev. B 40 (1989) 3616–3621, http://dx.doi.org/10.1103/PhysRevB.40.3616.
[24] Y. Wang, J. Wang, H. Zhang, V. Manga, S. Shang, L. Chen, Z. Liu, A first-principles approach to finite temperature elastic constants, J. Phys.: Condens. Matter 22 (22) (2010) 225404.
[25] A. Van de Walle, M. Asta, G. Ceder, The alloy theoretic automated toolkit: a user guide, Calphad 26 (4) (2002) 539–553.
[26] S. Wei, M. Chou, Ab initio calculation of force constants and full phonon dispersions, Phys. Rev. Lett. 69 (19) (1992) 2799.
[27] A. Van De Walle, G. Ceder, The effect of lattice vibrations on substitutional alloy thermodynamics, Rev. Modern Phys. 74 (1) (2002) 11.
[28] J.C. Slater, A simplification of the hartree-fock method, Phys. Rev. 81 (3) (1951) 385.
[29] M. Naguib, M. Kurtoglu, V. Presser, J. Lu, J. Niu, M. Heon, L. Hultman, Y. Gogotsi, M.W. Barsoum, Two-dimensional nanocrystals produced by exfoliation of Ti_3AlC_2, Adv. Mater. 23 (37) (2011) 4248–4253.
[30] E. Kisi, J. Crossley, S. Myhra, M. Barsoum, Structure and crystal chemistry of Ti_3SiC_2, J. Phys. Chem. Solids 59 (9) (1998) 1437–1443.
[31] A. Jain, S.P. Ong, G. Hautier, W. Chen, W.D. Richards, S. Dacek, S. Cholia, D. Gunter, D. Skinner, G. Ceder, et al., Commentary: the materials project: a materials genome approach to accelerating materials innovation, Apl Mater. 1 (1) (2013) 011002.
[32] A. Savin, R. Nesper, S. Wengert, T.F. Fässler, Elf: the electron localization function, Angew. Chem. Int. Edit. English 36 (17) (1997) 1808–1832.
[33] Y. Zhou, Z. Sun, X. Wang, S. Chen, Ab initio geometry optimization and ground state properties of layered ternary carbides Ti_3MC_2 (M = Al, Si and Ge), J. Phys.: Condens. Matter 13 (44) (2001) 10001.
[34] P. Finkel, M. Barsoum, T. El-Raghy, Low temperature dependencies of the elastic properties of Ti_4AlN_3, $Ti_3Al_{1.1}C_{1.8}$, and Ti_3SiC_2, J. Appl. Phys. 87 (2000) 1701–1703.
[35] J. Wang, Y. Zhou, Recent progress in theoretical prediction, preparation, and characterization of layered ternary transition-metal carbides, Ann. Rev. Mater. Res. 39 (2009) 415–443.
[36] R. Hill, The elastic behaviour of a crystalline aggregate, Proc. Phys. Soc. Sect. A 65 (5) (1952) 349.
[37] J.-Y. Wang, Y.-C. Zhou, Polymorphism of Ti_3SiC_2 ceramic: first-principles investigations, Phys. Rev. B 69 (14) (2004) 144108.
[38] H. Zhang, X. Wu, K.G. Nickel, J. Chen, V. Presser, High-pressure powder X-ray diffraction experiments and ab initio calculation of Ti_3AlC_2, J. Appl. Phys. 106 (1) (2009) 013519.
[39] S. Zinkle, 7.3 Physical and Thermal Mechanical Characterization of Non-Irradiated Max Phase.
[40] T. Scabarozi, S. Amini, O. Leaffer, A. Ganguly, S. Gupta, W. Tambussi, S. Clipper, J. Spanier, M. Barsoum, J. Hettinger, et al., Thermal expansion of select M n AX n M = early transition metal, A = A group element, X = C or N phases measured by high temperature X-ray diffraction and dilatometry, J. Appl. Phys. 105 (2009) 013543.
[41] M.K. Drulis, A. Czopnik, H. Drulis, M. Barsoum, Low temperature heat capacity and magnetic susceptibility of Ti_3SiC_2, J. Appl. Phys. 95 (2004) 128–133.
[42] M. Ali, A. Islam, M. Hossain, F. Parvin, Phase stability, elastic, electronic, thermal and optical properties of $Ti_3Al_{1-x}Si_xC_2$ ($0 \leqslant x \leqslant 1$): First principle study, Phys. B: Condens. Matter 407 (21) (2012) 4221–4228.